第39卷第6期 无 机 化 学 学 报 Vol.39 No.6
2023年6月 CHINESE JOURNAL OF INORGANIC CHEMISTRY 1151-1158

一种水中稳定的锌(Ⅱ)金属有机骨架用于检测四环素

王 璇 王记江* 唐 龙* 王劳棒 岳二林 白 超 王 潇 张玉琦
(延安大学化学与化工学院,延安市新能源新功能材料重点实验室,
陕西省化学反应工程重点实验室,延安 716000)

摘要: 采用溶剂热法合成1个锌(Ⅱ)金属有机骨架(Zn-MOF):$[Zn(H_2L)(4,4'\text{-bpy})]_n$ (**1**),其中H_4L=1,1′-乙烷基联苯-3,3′,5,5′-四羧酸,4,4′-bpy=4,4′-联吡啶。通过单晶X射线衍射、元素分析和热重分析等方法对其结构进行表征。单晶结构分析表明,**1**属于单斜晶系*C*2/*c*空间群,H_2L^{2-}配体采取单齿配位模式连接Zn(Ⅱ)形成一维链,4,4′-bpy连接一维链构筑成二维波浪状网。该化合物在水中表现出良好的稳定性,并且可作为高灵敏度、高选择性荧光探针检测四环素(TET),其检出限为0.17 μmol·L^{-1}。**1**可成功用于延河水中TET的测定。此外,还研究了**1**对TET的荧光猝灭机理。

关键词: 金属有机骨架; 晶体结构; 四环素; 荧光传感器
中图分类号: O614.24+1 **文献标识码:** A **文章编号:** 1001-4861(2023)06-1151-08
DOI: 10.11862/CJIC.2023.069

A stable Zinc(Ⅱ) metal-organic framework in water for the detection of tetracycline

WANG Xuan WANG Ji-Jiang* TANG Long* WANG Lao-Bang
YUE Er-Lin BAI Chao WANG Xiao ZHANG Yu-Qi
(*Yan'an City Key Laboratory of New Energy & New Functional Materials, Shaanxi Key Laboratory of Chemical Reaction Engineering, College of Chemistry and Chemical Engineering, Yan'an University, Yan'an, Shaanxi* 716000, *China*)

Abstract: A Zinc(Ⅱ) metal-organic framework (Zn-MOF), namely $[Zn(H_2L)(4,4'\text{-bpy})]_n$ (**1**), where H_4L=1,1′-ethylbiphenyl-3,3′,5,5′-tetracarboxylic acid, 4,4′-bpy=4,4′-bipyridine, was successfully synthesized under solvothermal conditions. The structure was characterized by single-crystal X-ray diffraction, elemental analysis, and thermogravimetric analysis. The single crystal structure analysis shows that **1** belongs to the monoclinic *C*2/*c* space group and H_2L^{2-} ligands adopt monodentate coordination mode, connecting with Zn(Ⅱ) to form 1D chains. Finally, the 1D chains are connected by 4,4′-bpy to form a 2D wavelike network. **1** shows good stability in water, and can be used as a highly sensitive and selective fluorescent probe to detect tetracycline (TET) with a detection limit of 0.17 μmol·L^{-1}. **1** can be successfully used for the determination of tetracycline in Yanhe River water. In addition, the possible fluorescence quenching mechanisms of **1** were also studied. CCDC: 2212375, **1**.

Keywords: metal-organic framework; crystal structure; tetracycline; fluorescent sensor

In recent years, the emergence of antibiotics as a new class of organic pollutants in the natural water environment has attracted extensive attention from domestic scholars. Tetracycline (TET) antibiotics are one of the most widely used antibiotics in China due to their low cost and low toxicity. They have a high half-life in water. They often accumulate in trace form in water, and enter mammals through drinking water and

收稿日期:2022-12-24。收修改稿日期:2023-03-18。
国家自然科学基金(No.21373178)、陕西省自然科学基础研究计划(No.2021JQ-614)、陕西省教育厅自然科学基金(No.21JK0978)、陕西省大学生创新创业训练计划项目(No.S202210719086)资助。
*通信联系人。E-mail:yadxwjj@126.com,ydtanglong@163.com;Tel(Fax):0911-2332037

the food chain, causing liver damage, increasing drug resistance, and threatening environmental safety[1]. Therefore, it is of great significance to study the detection of TET.

Metal-organic frameworks (MOFs) are porous materials that have recently attracted a great deal of attention due to their high potential for use in molecule design[2-3]. These materials are constructed from inorganic clusters and organic molecules to form 1D, 2D, or 3D structures. Due to its many advantages, MOFs have been successfully applied in fields such as heterogeneous catalysis[4-7], gas storage and separation[8-10], drug delivery[11], sensing[12-13], energy storage[14], and conductivity[15]. A large number of MOFs with luminescent sensing properties were synthesized and used for the detection of specific metal ions, small organic molecules, antibiotics, and nitroaromatic compounds (NACs)[16-18]. Especially, the MOFs of transition metal ions with d^{10} electronic structure have better luminescence properties, because the metal ions may shift and enhance the emission of organic ligands[19-21].

Herein, we report a new MOF, which was constructed with 1,1′-ethylbiphenyl-3,3′, 5,5′-tetracarboxylic acid (H_4L), 4,4′-bipyridine (4,4′-bpy) as well as Zn(Ⅱ) ion, namely $[Zn(H_2L)(4,4'\text{-bpy})]_n$ (**1**). It has good stability and fluorescence properties in water and can be used as a highly sensitive and selective fluorescence probe to detect TET with a detection limit of 0.17 μmol·L^{-1}. In addition, the fluorescence quenching mechanism of **1** is also discussed in detail.

1 Experimental

1.1 Reagents and instruments

All reagents and solvents were commercially available and used directly without further purification. The C, H, and N elemental analyses were conducted with a PerkinElmer PE-2400 elemental analyzer. The crystal data were collected on a Bruker SMART APEX-Ⅱ single-crystal X-ray diffractometer. Powder X-ray diffraction (PXRD) patterns were recorded with a Bruker D8 ADVANCE diffractometer operating at 40 kV and 40 mA using Cu $K\alpha$ radiation (λ=0.154 18 nm) at a scanning rate of 2 (°)·min^{-1} from 5° to 50°. Thermal gravimetric analysis (TGA) was performed with a NETZSCH STA 449F3 thermal gravimetric analyzer in flowing nitrogen at a heating rate of 10 ℃·min^{-1}. The UV-Vis spectra were measured using a UV-2700 spectrophotometer. Fluorescence experiments were carried out on a Hitachi F-7100 Fluorescence Spectrophotometer.

1.2 Synthesis of MOF 1

A mixture of $Zn(NO_3)_2·6H_2O$ (0.1 mmol, 0.029 7 g), H_4L (0.05 mmol, 0.017 9 g), and 4,4′-bpy (0.05 mmol, 0.007 8 g) were dissolved in a mixed solvent of DMF (3 mL), H_2O (3 mL), and HNO_3 (0.1 mL, 6 mol·L^{-1}). And then the mixed solution was placed in a 10 mL glass bottle and reacted at 95 ℃ for 3 d. Finally, colorless bulk transparent crystals were obtained. Yield: 47% (based on Zn). Anal. Calcd. for $C_{28}H_{20}N_2O_8Zn$(%): C, 58.15; H, 3.46; N, 4.85. Found (%): C, 58.21; H, 3.45; N, 4.64.

1.3 Crystal structure determination

The crystal with regular shape and moderate size was selected, and the single crystal data of **1** were collected on the Bruker SMART APEX-Ⅱ diffractometer (Mo $K\alpha$ radiation and λ=0.071 073 nm). The diffraction data were corrected by semi-empirical absorption using the SADABS program. The crystal structure was solved using direct methods and then refined by the full-matrix least-squares techniques on F^2 using SHELXL. All non-hydrogen atoms were refined anisotropically. The crystallographic data of MOF **1** is shown in Table 1. Selected bond lengths and bond angles are listed in Table 2.

CCDC: 2212375, **1**.

Table 1 Crystal data and structure refinement parameters for 1

Parameter	1	Parameter	1
Formula	$C_{28}H_{20}N_2O_8Zn$	V / nm^3	2.398 1(6)
Formula weight	577.81	Z	4
Crystal system	Monoclinic	D_c / (g·cm^{-3})	1.595
Space group	$C2/c$	F(000)	1 176

Continued Table 1

a / nm	2.029 1(3)	Goodness-of-fit (on F^2)	1.021
b / nm	1.0105 5(14)	R_1, wR_2 [$I>2\sigma(I)$]	0.038 5, 0.092 5
c / nm	1.419 233(19)	R_1, wR_2 (all data)	0.049 1, 0.098 4
β / (°)	124.508(2)		

Table 2　Selected bond lengths (nm) and angles (°) for 1

Zn1—O1	0.197 93(16)	Zn1—O1A	0.197 93(16)	Zn1—N1	0.207 03(18)
Zn1—N1A	0.207 04(18)				
O1—Zn1—O1A	13.803(11)	O—Zn1—N1	10.786(7)	O1A—Zn1—N1	9.937(7)
O—Zn1—N1A	9.937(7)	O1A—Zn1—N1A	10.786(7)	N1—Zn1—N1A	9.807(10)

Symmetry code: A: 1−x, y, 0.5−z.

2　Results and discussion

2.1　Crystal structure

MOF **1** crystallizes in the monoclinic crystal system with the $C2/c$ space group. The asymmetric unit of **1** consists of one Zn(Ⅱ) ion, one H_2L^{2-} ligand, and one 4,4′-bpy ligand. As shown in Fig.1a, each Zn(Ⅱ) is four-coordinated by two O atoms (O1, O1A) from two different H_2L^{2-} ligands, two nitrogen atoms (N1, N1A) from 4,4′-bpy ligands. All the Zn—O (0.197 93 (16) nm) and Zn—N (0.207 03(18) - 0.207 04(18) nm) bond lengths fall into the normal ranges (Table 2). As shown in Fig. 1b, the single crystal structure analysis shows that H_2L^{2-} ligands adopt monodentate coordination mode, connecting with Zn(Ⅱ) to form 1D chains. Finally, the 1D chains are connected by 4,4′-bpy to form a 2D wavelike network.

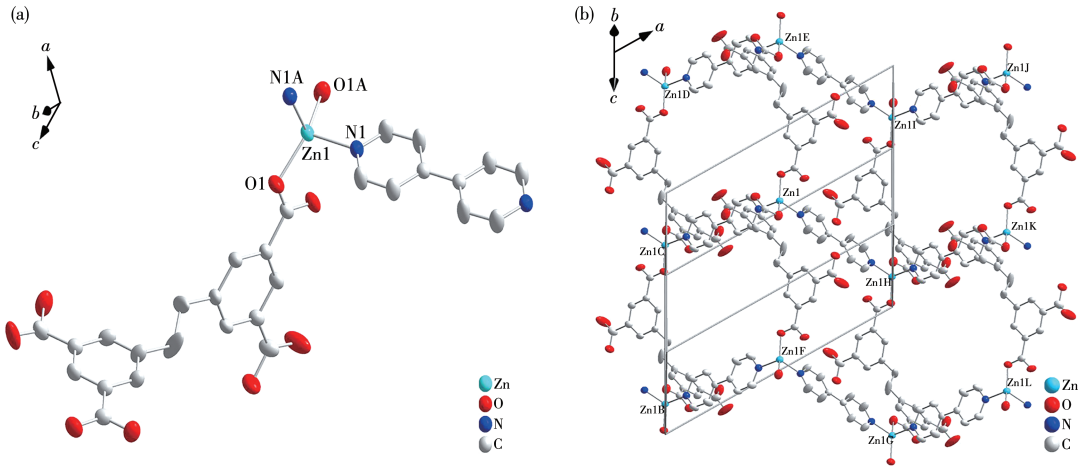

50% ellipsoid probability; Symmetry codes: A:1−x, y, 0.5−z; B: 0.5−x, 0.5−y, 1−z; C: 0.5−x, 0.5−y, −z; D: 0.5−x, 0.5−y, −1−z; E: x, y, −1−z; F: x, y,1+z; G: 1.5−x, 0.5−y, 2−z; H: 1.5−x, 0.5−y, 1−z; I: 1.5−x, 0.5−y, −z; J: 1+x, y, z; K: 1+x, y, 1+z; L: 1+x, y, 2+z

Fig.1　(a) Ellipsoid diagram of the molecular structure of MOF **1**; (b) 2D wavelike network of **1**

2.2　Thermal stability

To identify the thermal stability of MOF **1**, the TGA was performed. As shown in Fig.2, the weight loss of **1** was 12.1% before 110 ℃, which corresponds to the release of the free water. The 2D networks started to decompose upon further heating up to about 400 ℃.

2.3　Purity and skeleton stability

To confirm the purity of MOF **1**, the PXRD pattern of **1** was measured. The position of the diffraction peak in the PXRD experiment was consistent with those of single crystal structure simulation, implying the pure phase of **1** (Fig. 3). The skeleton is basically

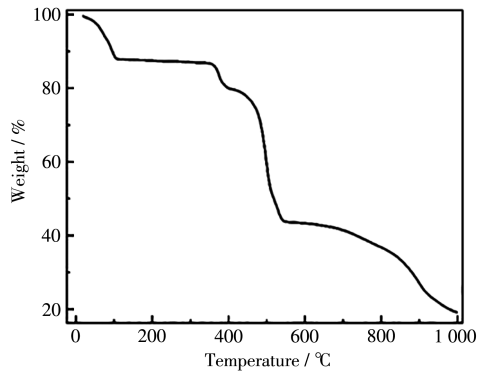

Fig.2 TGA curve of MOF **1**

unchanged when **1** was immersed in acidic and basic aqueous solutions for 24 h, indicating that **1** has good acid and alkali resistance (Fig.4).

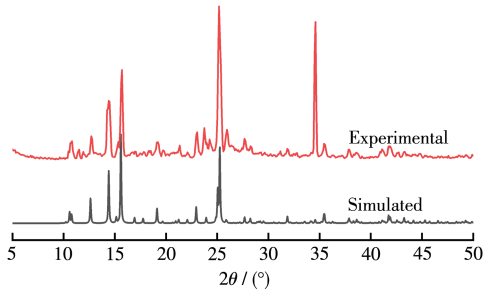

Fig.3 PXRD patterns of MOF **1**

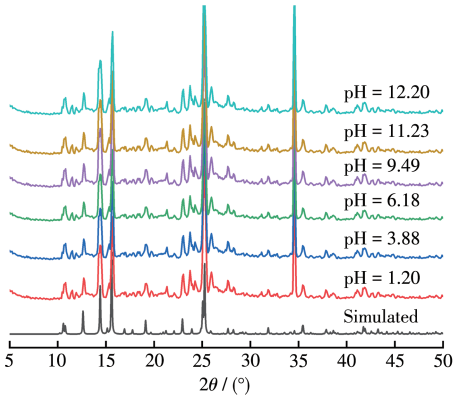

Fig.4 PXRD patterns of MOF **1** immersed in the aqueous solutions with different pH values for 24 h

2.4 Photoluminescence property

Due to the excellent luminescence properties of d^{10} metal MOFs, the luminescence of **1** and the H_4L ligand were investigated. As shown in Fig. 5, H_4L had an emission peak at 444 nm (λ_{ex}=362 nm). Compared to the fluorescence spectrum of the ligand, the fluorescence intensity of **1** was stronger than that of the ligand, which may be due to coordination interactions[22]. The emission spectrum of **1** had a partial redshift, which may be caused by the charge transfer between H_4L and Zn(Ⅱ)[23].

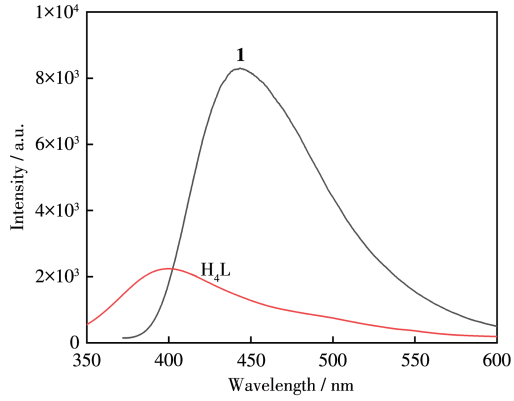

Fig.5 Solid luminescent spectra of MOF **1** and ligand H_4L

2.5 Antibiotics sensing

The wanton use of antibiotics has caused great pollution to the water system and environment. Therefore, it is very urgent for us to find a simple and efficient method to detect antibiotics[24]. Therefore, the luminescence sensing of **1** for different antibiotics was investigated, including lincomycin hydrochloride (LIN), metronidazole (MDZ), ornidazole (ODZ), TET, roxithromycin (ROX), chloramphenicol (CAP), gentamicin sulfate (GEN), azithromycin (AZM), cefixime (CEF) and penicillin sodium (PEN). As shown in Fig.6a, when TET was added, the fluorescence of **1** showed the maximum quenching. In the presence of other antibiotics, anti-interference experiments were carried out for TET. The experimental results showed that the fluorescence of **1** was also quenched to a large extent when TET was added in the presence of other antibiotics (Fig.6b). Subsequently, the quantitative experiment of TET was carried out. When the concentration of TET increased, the fluorescence intensity of **1** gradually decreased. When the concentration of TET reached 250 μmol·L^{-1}, the quenching efficiency of TET was as high as 97.97% (Fig. 6c). And I_0/I value was also linearly correlated with a low TET concentration (Fig. 6d). The detection limit was calculated using $3\sigma/k$ (σ: standard deviation, k: slope), and the detection limit for **1** towards TET was 0.17 μmol·L^{-1}. In addition, after four cycles, we found that the fluorescence intensity could still be restored to

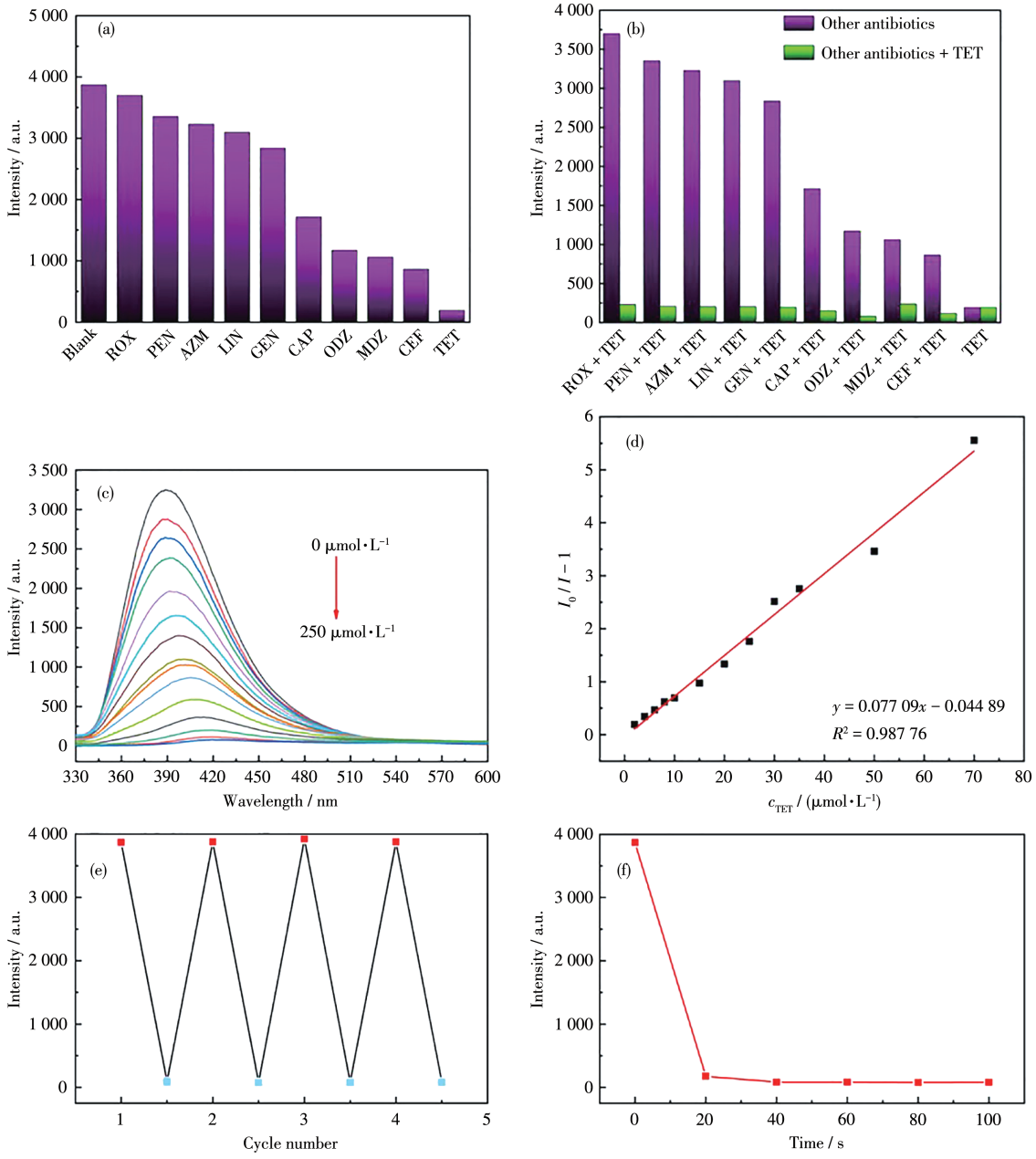

Fig.6　(a) Luminescent intensity of **1** in different antibiotics; (b) Luminescence intensity of **1** in mixed antibiotics; (c) Emission spectra of **1** with different concentrations of TET; (d) Stern-Volmer plot for MOF **1** detecting TET in low concentration; (e) Cycle stability of **1** for the detection of TET (red square: **1**, blue square: **1** + TET); (f) Effect of response time on the fluorescent intensities upon the addition of TET

the original intensity. **1** may be a recyclable fluorescent sensor (Fig. 6e). It was found that when TET of 250 μmol·L^{-1} was added, the luminescence intensities decreased rapidly and the fluorescence hardly changed after 20 s (Fig.6f).

2.6　Possible sensing mechanism

The reasons for fluorescence quenching that have been reported are as follows: (Ⅰ) the collapse and disintegration of the crystal framework, (Ⅱ) the mechanism of energy competition and absorption, (Ⅲ) the exchange of central metal ions, (Ⅳ) the mechanism of energy transfer, (Ⅴ) the mechanism of photoinduced electron transfer (PET)[25-31]. First of all, as shown in Fig.7, PXRD patterns of **1** were consistent with as-synthesized samples immersed in TET solution for 24 h, indicating that the crystal structure was intact. Therefore, framework col-

lapse is not the reason for fluorescence quenching. Secondly, because **1** detects antibiotics, it indicates that there is no metal ion exchange during fluorescence quenching. Another possible mechanism is energy allocation and transfer. We can see that there is a partial overlap between the emission spectrum of **1** and the UV absorption (300-400 nm) spectrum of TET (Fig.8). The reason for the fluorescence quenching of **1** may be due to energy absorption and energy transfer. Finally, the LUMO level of TET (−2.72 eV) is lower than **1** (Fig.9). The reason for fluorescence quenching may be that the electron transfers from the LUMO level of **1** to TET. At the same time, I_0/I value was also linearly correlated with low TET concentration (Fig.6d), indicating that the mechanism for fluorescence quenching should be more than one. When the concentration is low, it is linear, indicating that the competitive absorption is weak. With the increase in concentration, it is nonlinear, and the absorption also increases[32-34].

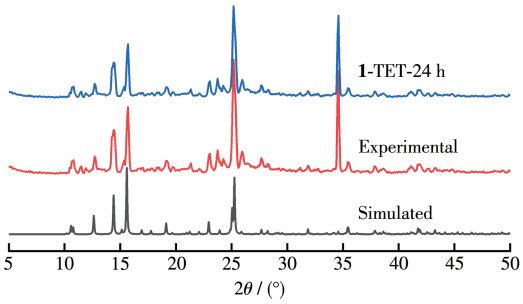

Fig.7 PXRD patterns of **1** and as-synthesized samples immersed in TET solution for 24 h

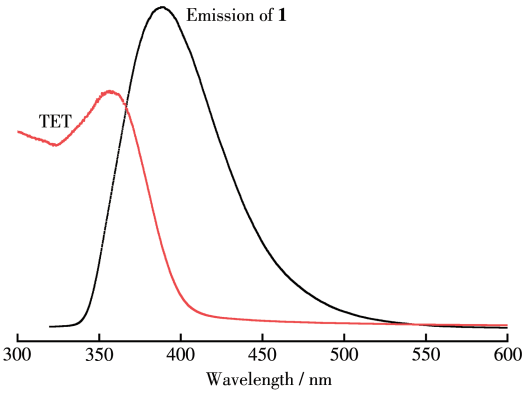

Fig.8 UV-Vis absorption spectrum of TET and emission spectrum of **1**

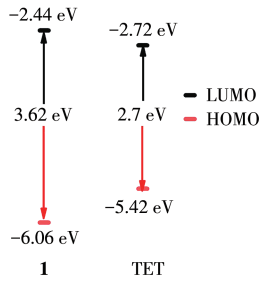

Fig.9 HOMO and LUMO energy levels of **1** and TET

2.7 Practical application in Yanhe River water

To prove the practicability of this method, TET was tested in Yanhe River water through the spiked recovery experiment. As shown in Table 3, the spiked recoveries at different concentrations were obtained, ranging from 94% to 103%. The relative standard deviation (RSD) values were 1.7% - 2.4%, indicating the reliability and practicability of **1** to detect TET in real samples.

Table 3 Recovery test of TET spiked in Yanhe River water samples

Spiked / (μmol·L^{-1})	Detected / (μmol·L^{-1})	RSD* / %	Recovery / %
0	Not detected	—	—
5	4.7	1.7	94
15	15.1	1.9	101
30	30.8	2.4	103

*n=3

3 Conclusions

In summary, a Zn-MOF (**1**) is successfully synthesized under solvothermal conditions. Structural analysis shows that **1** is a 2D wavelike network. It has high selectivity and sensitivity for the detection of TET by fluorescence quenching. Through the spiked recovery experiment, TET in the actual water samples along the river can also be detected. Finally, the sensing mechanism is discussed in detail. The cause of TET quenching might be energy resonance transfer or electron transfer.

Conflicts of interest: The authors declare no competing financial interest.

References:

[1]Bai Y H, Su J F, Wen Q, Li G Q, Xue L, Huang T L. Removal of tetra-

cycline by denitrifying Mn(Ⅱ)-oxidizing bacterium *Pseudomonas* sp. H117 and biomaterials (BMO and MBMO): Efficiency and mechanisms. *Bioresour. Technol.*, **2020**,**312**:123565

[2]Yaghi O M, O'Keeffe M, Ockwig N W, Chae, H K, Eddaoudi M, Kim J. Reticular synthesis and the design of new materials. *Nature*, **2003**, **423**:705-714

[3]Butova V V, Soldatov M A, Guda A A, Lomachenko K A, Lamberti C. Metal-organic frameworks: Structure, properties, methods of synthesis and characterization. *Russ. Chem. Rev.*, **2016**,**85**:280-307

[4]Liang Q N, Chen J M, Wang F L, Li Y W. Transition metal-based metal-organic frameworks for oxygen evolution reaction. *Coord. Chem. Rev.*, **2020**,**424**:213488

[5]Sakamoto N, Nishimura Y F, Nonaka T, Ohashi M, Ishida N, Kitazumi K, Kato Y, Sekizawa K, Morikawa T, Arai T. Self-assembled cuprous coordination polymer as a catalyst for CO_2 electrochemical reduction into C_2 products. *ACS Catal.*, **2020**,**10**(18):10412-10419

[6]Woldu A R, Huang Z L, Zhao P X, Hu L S, Astruc D. Electrochemical CO_2 reduction (CO_2RR) to multi-carbon products over copper-based catalysts. *Coord. Chem. Rev.*, **2022**,**454**:214340

[7]Zhou Y T, Abazari R, Chen J, Tahir M, Kumar A, Ikreedeegh R R, Rani E, Singh H, Kirillov A M. Bimetallic metal-organic frameworks and MOF-derived composites: Recent progress on electro and photoelectrocatalytic applications. *Coord. Chem. Rev.*, **2022**,**451**:214264

[8]Lin J B, Zhang J P, Chen X M. Nonclassical active site for enhanced gas sorption in porous coordination polymer. *J. Am. Chem. Soc.*, **2010**, **132**:6654-6656

[9]Duan J G, Jin W Q, Kitagawa S. Water-resistant porous coordination polymers for gas separation. *Coord. Chem. Rev.*, **2017**,**332**:48-74

[10]Duan J G, Higuchi M, Krishna R, Kiyonaga T, Tsutsumi Y, Sato Y, Kubota Y, Takata M, Kitagawa S. High $CO_2/N_2/O_2$/CO separation in a chemically robust porous coordination polymer with low binding energy. *Chem. Sci.*, **2014**,**5**(2):660-666

[11]Imaz I, Rubio-Martinez M, Garcia-Fernandez L, Garcia F, Ruiz-Molina D, Hernando J, Puntes V, Maspoch D. Coordination polymer particles as potential drug delivery systems. *Chem. Commun.*, **2010**,**46**: 4737-4739

[12]Dutta B, Hazra A, Dey A, Sinha C, Ray P P, Banerjee P, Mir M H. Construction of a succinate-bridged Cd(Ⅱ)-based two-dimensional coordination polymer for efficient optoelectronic device fabrication and explosive sensing application. *Cryst. Growth Des.*, **2020**, **20**(2): 765-776

[13]Wen T, Zhang D X, Liu J, Lin R, Zhang J. A multifunctional helical Cu(I) coordination polymer with mechanochromic, sensing and photocatalytic properties. *Chem. Commun.*, **2013**,**49**:5660-5662

[14]Luo X Z, Abazari R, Tahir M, Fan W K, Kumar A, Kalhorizadeh T, Kirillov A M, Amani-Ghadim A R, Chen J, Zhou Y T. Trimetallic metal-organic frameworks and derived materials for environmental remediation and electrochemical energy storage and conversion. *Coord. Chem. Rev.*, **2022**,**461**:214505

[15]Horike S, Umeyama D, Kitagawa S. Ion conductivity and transport by porous coordination polymers and metal-organic frameworks. *Acc. Chem. Res.*, **2013**,**46**(11):2376-2384

[16]陈小莉, 刘露, 商璐, 蔡苗, 崔华莉, 杨华, 王记江. 一种高灵敏、多响应的Zn-MOF荧光传感器对Fe^{3+}、2,4,6-三硝基苯酚和奥硝唑的检测. 无机化学学报, **2022**,**38**(4):735-744
CHEN X L, LIU L, SHANG L, CAI M, CUI H L, YANG H, WANG J J. A highly sensitive and multi-responsive Zn-MOF fluorescent sensor for detection of Fe^{3+}, 2,4,6-trinitrophenol, and ornidazole. *Chinese J. Inorg. Chem.*, **2022**,**38**(4):735-744

[17]张龄文, 刘淑芹, 张佩佩, 倪爱云, 张建军. 一例基于5-((萘-1-基甲基)氨基)间苯二甲酸配体的Cd(Ⅱ)金属有机骨架的合成、晶体结构及对酸性氨基酸的检测. 无机化学学报, **2022**,**38**(9):1871-1877
ZHANG L W, LIU S Q, ZHANG P P, NI A Y, ZHANG J J. Synthesis, crystal structure, and detection of acidic amino acids of a Cd(Ⅱ) metal-organic framework based on 5-((naphthalen-1-ylmethyl) amino) isophthalic acid. *Chinese J. Inorg. Chem.*, **2022**,**38**(9):1871-1877

[18]徐涵, 潘兆瑞, 亓昭鹏, 孙洁. 基于V型配体的三个荧光Zn-MOF对水溶液中2,4,6-三硝基苯酚和Fe^{3+}的荧光传感. 无机化学学报, **2022**,**38**(12):2479-2490
XU H, PAN Z R, QI Z P, SUN J. Three luminescent Zn-MOFs based on V-shaped ligands for fluorescence sensing of 2,4,6-trinitrophenol and Fe^{3+} in aqueous solution. *Chinese J. Inorg. Chem.*, **2022**,**38**(12): 2479-2490

[19]Wang S Q, Wang L, Zhu Y M, Song Y H. Fluorescent detection of S^{2-} based on ZnMOF-74 and CuMOF-74. Spectroc. *Acta Pt. A-Molec. Biomolec. Spectr.*, **2020**,**236**:118327

[20]Farahani Y D, Safarifard V. Highly selective detection of Fe^{3+}, Cd^{2+} and CH_2Cl_2 based on a fluorescent Zn-MOF with azine-decorated pores. *J. Solid State Chem.*, **2019**,**275**:131-140

[21]Chandrasekhar P, Mukhopadhyay A, Savitha G, Moorthy J N. Remarkably selective and enantiodifferentiating sensing of histidine by a fluorescent homochiral Zn-MOF based on pyrene-tetralactic acid. *Chem Sci.*, **2016**,**7**:3085-3091

[22]Gogia A, Mandal S K. A rational design and green synthesis of 3D metal organic frameworks containing a rigid heterocyclic nitrogen-rich dicarboxylate: Structural diversity, CO_2 sorption and selective sensing of 2,4,6-TNP in water. *Dalton Trans.*, **2019**,**48**:2388-2398

[23]Liu T Y, Qu X L, Zhang Y, Yan B. A stable Cd(Ⅱ)-based metal-organic framework: Synthesis, structure, and its Eu^{3+} functionalization for ratiometric sensing on the biomarker 2-(2-methoxyethoxy) acetic acid. *Inorg. Chem.*, **2021**,**60**(12):8613-8620

[24]Wang L B, Wang J J, Yue Er L, Li J F, Tang L, Bai Ch, Wang X, Hou X Y, Zhang Y Q. Information encryption, highly sensitive detection of nitrobenzene, tetracycline based on a stable luminescent Cd-MOF. Spectroc. *Acta Pt. A-Molec. Biomolec. Spectr.*, **2022**,**269**: 120752

[25]Dang S, Ma E, Sun Z M, Zhang H J. A layer-structured Eu-MOF as a highly selective fluorescent probe for Fe^{3+} detection through a cation-exchange approach. *J. Mater. Chem. C*, **2012**,**22**:16920-16926

[26]Chen Z, Sun Y W, Zhang L L, Sun D, Liu F L, Meng Q G, Wang R M, Sun D F. A tubular europium-organic framework exhibiting selec-

tive sensing of Fe^{3+} and Al^{3+} over mixed metal ions. *Chem. Commun.*, **2013**,**49**:11557-11559

[27]Zhao X L, Tian D, Gao Q, Sun H W, Xu J, Bu X H. A chiral lanthanide metal-organic framework for selective sensing of Fe(Ⅲ) ions. *Dalton Trans.*, **2016**,**45**:1040-1046

[28]Nagarkar S S, Joarder B, Chaudhari A K, Mukherjee S, Ghosh S K. Highly selective detection of nitro explosives by a luminescent metal-organic framework. *Angew. Chem. Int. Ed.*, **2013**,**52**(10):2881-2885

[29]Pramanik S, Zheng C, Zhang X, Emge T J, Li J. New microporous metal-organic framework demonstrating unique selectivity for detection of high explosives and aromatic compounds. *J. Am. Chem. Soc.*, **2011**,**133**(12):4153-4155

[30]Liu Z P, He W J, Guo Z J. Metal coordination in photoluminescent sensing. *Chem. Soc. Rev.*, **2013**,**42**:1568-1600

[31]He T S, Lan Y L, Li Z Y, Zhu L N, Li X Z. Chiral coordination polymers from a new 2-deoxy-*D*-ribose derivative linker: Syntheses, structures, and Fe^{3+} fluorescent probe functions. *Cryst. Growth Des.*, **2021**,**21**(4):2233-2242

[32]Huang Y, Qin Y, Ge Y, Cui Y F, Zhang X M, Li Y H, Yao J L. Rationally assembled nonanuclear lanthanide clusters: Dy_9 displays slow relaxation of magnetization and Tb_9 serves as luminescent sensor for Fe^{3+}, CrO_4^{2-} and $Cr_2O_7^{2-}$. *New J. Chem.*, **2019**,**43**:19344-19354

[33]Smith J A, Singh-Wilmot M A, Carter K P, Cahill C L, Ridenour J A. Lanthanide-2,3,5,6-tetrabromoterephthalic acid metal-organic frameworks: Evolution of halogen···halogen interactions across the lanthanide series and their potential as selective bifunctional sensors for the detection of Fe^{3+}, Cu^{2+}, and nitroaromatics. *Cryst. Growth Des.*, **2019**,**19**(1):305-319

[34]Chen S, Yu Y L, Wang J H. Inner filter effect-based fluorescent sensing systems: A review. *Anal. Chim. Acta*, **2018**,**999**:13-26